Nanotechnology Perceptions
ISSN 1660-6795
www.nano-ntp.com

Experimental Study of Abrasive Wear Behavior of Pr_6O_{11} Modified WC-12Co Coatings Deposited by HVOF Technique

Satyanarayan Dubey[1], Shyam Birla[1], Tribhuwan Kishore Mishra[2]

[1]Department of Mechanical Engineering, Oriental University, Indore, India
[2]Department of Mechanical Engineering, GGITS, Jabalpur, India
Email: satyanarayan.hcet@gmail.com

Decarburization and decomposition are critical issues that degrade the WC-12Co coating deposited by the HVOF technique. To overcome this issue, this experimental work investigates the effect of adding praseodymium oxide (Pr6O11) on the dry abrasive wear behaviour of WC-12Co HVOF sprayed coatings. Several features of the coatings were thoroughly studied, including microstructure, phase conformation, microhardness, porosity, adhesive and bond strength. The result exhibits that the addition of Pr6O11 refines the grain structure by decreasing the grain size. XRD analysis indicates that Pr6O11 reduces the decarburization by restricting the formation of W2C phase. The 2 Pr6O11 modified coating shows higher microhardness and adhesive bond strength, which were 7.3% and 6.9% higher than the conventional WC-12Co coating, respectively. The modified coating exhibits a lower specific wear rate and lower coefficient of friction due to the lubricating properties of rare earth oxide. 2 wt. % Pr6O11 modified coating shows 40% higher than WC-12Co coating. Different wear mechanisms of modified coatings are discussed in this paper.

1. Introduction

Coating deposition has remarkable wear resistance and has attracted substantial interest in recent years for its capacity to safeguard mechanical components under critical working circumstances. Because of their outstanding wear, friction, and mechanical qualities, these coatings are widely used in a variety of industrial applications, including automotive, aerospace, petrochemical, and agriculture[1]. Thermally sprayed techniques have been widely used for coating deposition, which includes High-velocity oxy fuel (HVOF), plasma spray, High-velocity air fuel (HVAF), and detonation gun coating [2]. The high-velocity oxy-fuel coating offers low porosity, low decomposition rate, higher hardness, and better bond strength. Tungsten carbide-based coatings are used extensively in industries due to their good tribological properties even at higher temperatures [3-4]. Types of binder phase, melting temperature, spraying velocity, grain size, and feedstock powder quality influence the microstructural and wear properties [5]. The WC-12Co also exhibits excellent mechanical and

microstructural properties [7-8]. Cobalt is extensively used in tungsten carbide, increasing the hardness, toughness, and higher bonding strength and offering greater microstructural properties [9-10].

Due to the high heat addition and kinetic energy, semi-molten and molten particles form multilayered formations when sprayed into the substrate during the HVOF spraying process. This multilayered structure is rapidly cooled and quenched, resulting in a brittle structure and the disintegration of WC into the amorphous phase W_2C [11-12]. This change to W_2C occurs due to WC disintegration in flight, with the breakdown material generating W_2C that is trapped as an amorphous phase during fast solidification. During abrasive wear, the W_2C amorphous phase produces microcracks at the WC-Co interfaces, primarily when strain hardening occurs in the Co binder. As a result, Co binder undergoes strain hardening and the Co binder may be partially removed, causing WC particles to be pushed away from the coated surface. In extremely abrasive and erosive wear conditions with constant tangential and radial stresses, eliminating pulled-out particles and fortifying the WC-Co interface are crucial [9].

The W_2C phase likewise influences hardness and bond strength and also promotes crack formation. [13-15]. This results in the cobalt binder's detachment; thus, a series of carbide particles are removed from the matrix [11-12].

Recently, more effort has been focused on minimizing the decarburization and decomposition of WC-12Co by adding rare earth elements. Various studies have revealed that the addition of an optimum amount of rare earth elements into the coating had a major change in the tribological and mechanical properties [16-17]. The rare-earth element restricts the boundary segregation, refines the microstructure, acts as an interface between WC and Co, and remains stable even at higher temperatures [18-19]. Rare earth promotes the formation of an outside layer and increases the adhesive bond strength. Various researchers have added cerium oxide and lanthanum oxide to nickel-based coatings and reported that rare earth elements extensively improve grain structure boundaries and enhance wear resistance and hardness [20-23]. Praseodymium oxide endorses the nucleation of the particle as mixed cores. During precipitation, praseodymium oxide remains stable, whereas some parts respond with carbon and form rear earth carbides after melting. Thus, both formed heterogeneous microstructure and increased the density of carbide particles that existed in the matrix[24]

Because of its lower melting point, Co binder melts first in the WC-Co matrix and immediately connects carbide particles to the substrate during the coating process. Oxygen carbide particles dissolve instantly in the molten Co binder when oxygen interacts with the carbide grain, and subsequently, decarburization of carbide occurs. Rare earth distributes along the grain boundary and reinforces it when it is combined with WC-CO and absorbed by the WC-Co dual phase due to its high surface energy. Therefore, some part of Co is retained on the border while some part melts hence, the contact area between the carbide particles and the oxy-acetylene flame decreases; eventually, decarburization falls dramatically from WC to W2C phase [17-19].

Praseodymium oxide forms hydroxide and oxide thin films to increase corrosion resistance [25]. Praseodymium oxide refines the microstructure and prevents crack formation [26]. Information on the effect of Pr_6O_{11} addition in WC-12Co coating on abrasive wear property is rare. Prior studies are based on the effect of Pr_6O_{11} on corrosion wear behaviour. The effect of

Pr_6O_{11} on abrasive wear behaviour, microstructural properties, and mechanical properties has not been investigated.

This work aims to examine the effect of Pr_6O_{11} addition on the tribological properties of WC-Co coatings under abrasive wear circumstances concerning microstructural and other mechanical properties.

2. Materials and experimental procedures

2.1 Sample preparation and Coating deposition

The current investigation selected commercially agglomerated and sintered WC- 12Co (WOKA 3102) powder with a particle size of 45 ±15 μm of 99.9% purity for coating deposition. The WC-12 Co powder was provided by MECPL, Jodhpur (India), and this powder was further modified by mixing Praseodymium oxide (Pr_6O_{11}), having a particle size of 1.0 to 4.6 microns (99.9% pure) procured from Star Minerals Mumbai (India). The specification of Praseodymium oxide powder is 0.010% La_2O_3, 0.050 % Nd_2O_3, 0.030 % CeO_2, 0.010 % Sm_2O_3, 100 ppm Fe, 100 ppm sodium and 99.9 % Pr_6O_{11}. Varying weight percentages (1, 2, and 3 wt. %) of Pr_6O_{11} powder were mixed with WC-12Co powder by mechanical mixing using ball mill grinder at a speed of 200 RPM for 1 hour in a forward and for one hour in a backward direction in the absence of any other media[19]. Circular coated samples of size Ø 12 mm × 5 mm were used for Sem and XRD examination.

These WC-12Co and Pr_6O_{11} modified coatings powders were deposited on circular cross section of AISI 1020 low carbon grade steel cylindrical substrates of size Ø 12 mm × 22 mm lengths. The high-velocity oxy-fuel (HVOF) coatings method was applied using the HVOF coating gun system (model HVOF HIPO JET2700, MEC, India) at M/S MECPL, Jodhpur (India). Coating thickness was targeted at 300±20 μm throughout the spraying. Prior to coating, powders were preheated in an electric muffle furnace for one hour to eliminate precipitate impurities and moisture. Prior to coating spraying, the cylindrical substrate was cleaned to remove foreign impurities and subsequently grit blasted using Al_2O_3 of size 650±40 μm at 90° blasting nozzle angle with a blasting pressure of 5 kg-cm^{-2} to increase the adhesion between substrate and coating [27]. Cylindrical specimens were pressed against a rotating polished disc by applying a small load for a certain period to ensure the perfect flatness of the surface. Coating parameters are shown in Table 1.

Table 1 Coating deposition Parameters

Parameter	Value
Oxygen Pressure (kg/sq.c)	10
Oxygen flow (slpm)	260 to 270
LPG pressure (kg/sq.cm)	7
LPG flow (slpm)	60 to 65
Air pressure (kg/sq.cm)	6
Air flow (slpm)	600
Powder feed rate (g/min)	45

Powder disc (rpm)	6
Nitrogen carrier gas flow (scfh)	20
Carrier gas pressure (kg/sq.cm)	5 to 6
Working distance (inch)	7

2.2 Characterization

Coated specimens prepared for metallographic examination were ground successively with silicon carbide emery paper of 220, 600, and 1200 grit sizes and then cloth polished using alumina paste. The etching was done as per ASTM B657 standard.

Feedstock powder and polished coated specimens were examined in the scanning electron microscope (JSM-6390LV, Jeol, Japan) along with coatings' energy dispersive spectroscopy (EDS) to reveal microstructural characteristics and elemental composition. The confirmation of phase of feedstock powder and coated samples were studied using Rigaku Smart Lab, 9 kW, X-ray diffractometer with Cu-Kα radiation of wavelength 1.5406Å.

The porosity of the coated surfaces was determined by examining SEM images through Image-J software, the area percentage counting method. Microhardness of the cross-section was measured using a Vickers indenter as per ASTM E384-2016 standard at 300 gm load for a dwell time of 15 seconds [22]. The average readings of three tests have been considered for evaluation of the coating hardness.

Adhesive bond strength was measured using a tensile testing machine (INSTRON) according to ASTM C633-2013 standard of coated sample size Ø 25.1 mm × 38.1 mm at room temperature 25± 2°C incorporating epoxy resin adhesive. Averages readings of three tests were taken to evaluate the adhesive bond strength. The surface roughness of coated specimens was measured through a profilometer (Surftest SJ-210 Mitutoyo make, Japan). The stylus's tip radius and tip angle were 2μm and 90°, respectively.

2.2 Abrasive wear test

An abrasive wear test was performed on a pin-on-disc wear tester (Model TE-165, Megnum, India) in conformity with ASTM G-99-5 standard, as shown in Fig. 1. Coated polished pin specimens of size Ø12 mm ×22 mm lengths were used for the tests. Commercially available branded silicon carbide (400 μm sized comprising angular shape) paper was used as abrasive media, mounted on steel disc of size Ø165 mm × 6 mm by using adhesive glue. Wear (micron), and the coefficient of friction (COF) are continuously measured using a linear variable displacement transducer (LVDT) attached to a pin-on-disc wear tester. Lab view software is used to record the COF. All the tests were carried out at room temperature. The temperature of the pin and abrasive media was measured by two thermocouples situated 5 mm apart. The mass-loss method was used to measure the wear using an electronic weighing machine (DELMER electronic balance) with an accuracy of 0.0001mg. Wear rate was presented in terms of specific wear rate (mm^3/Nm). Samples were cleaned with acetone before and after each test. The coefficient of friction (COF) was constantly recorded. The wear test was performed at two different loads, 20N and 40N. The load is applied on the load pan and transferred to the pin abrasive media interface through the cantilever mechanism. The worn-out surfaces were investigated under SEM after cleaning in an ultrasonic bath. Wear test

parameters are given in Table 2.

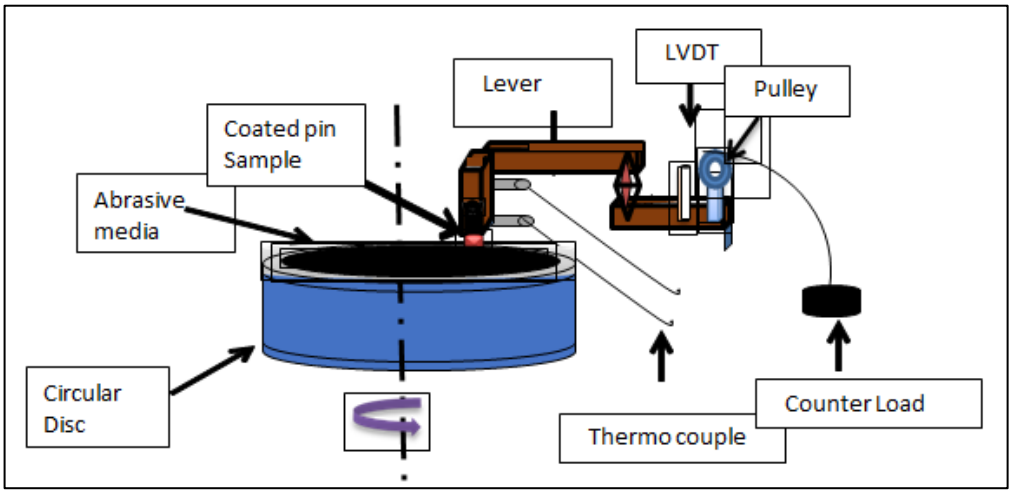

Fig. 1 Schematic diagram of pin-on-disc friction and wear test rig

Table 2 Wear Test Parameters

Parameter	Value
Average velocity	1.0 m/sec
Track radius	60 mm
Sliding Distance	1200 m
Applied Load	20 N, 40 N

3. Results and discussion

3.1 Powder and coating characterization

The scanning electron microscope images of unmodified and modified feedstock powder are shown in Fig. 2 (a-d). The powder retains a spherical shape and gets accumulates to Co binder particles [23]. The WC-12Co powder exhibited a pore structure, and the Pr_6O_{11} modified powder showed a dense structure because Pr_6O_{11} dispersed and was retained outside the spherical boundary of the powder. The addition of Pr_6O_{11} makes the structure dense, as seen in Fig. 2(b-d), resulting in good flowability and decreasing resistance among powder particles during spraying. The change of powder size has been observed in Pr_6O_{11} modified coatings due to fracture of the agglomerated/ sintered feedstock and reduces the porosity of powder.

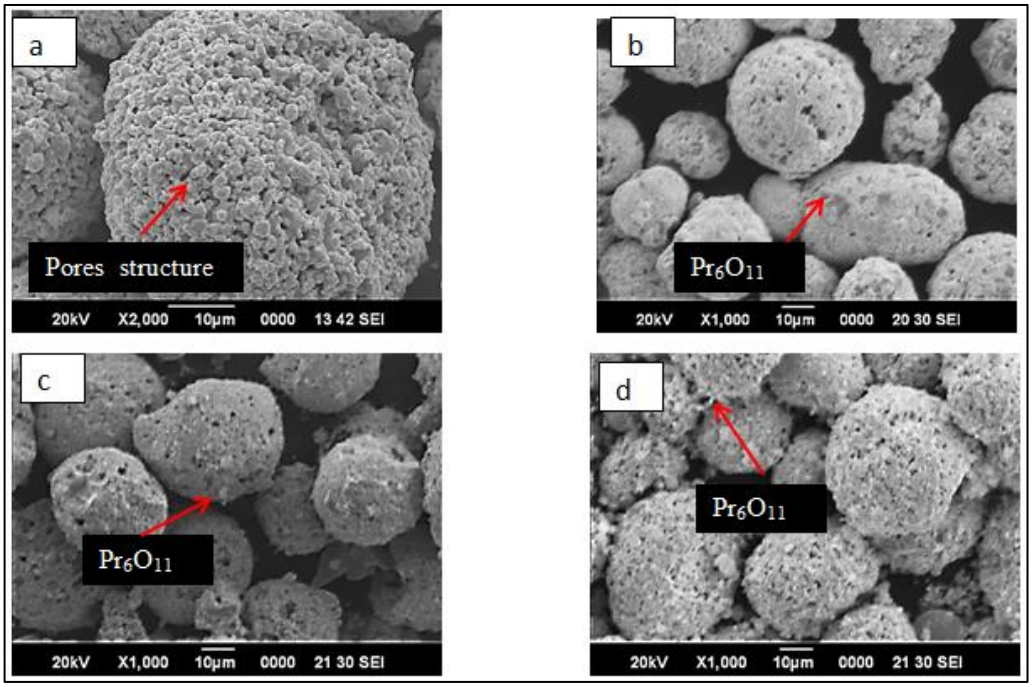

Fig. 2 SEM images of feedstock powder, (a) WC-12Co (b) 1Pr6O11modified (c)1.2 Pr_6O_{11} and (d) 1.8 Pr_6O_{11} modified

X-ray diffraction patterns of feedstock powder are shown in Fig. 3. Primary peaks of WC and secondary peaks of Co and Pr_6O_{11} confirm their presence in feedstock powder. It is difficult to identify peaks of Pr_6O_{11} in 0.6 Pr_6O_{11}, 1.2 Pr_6O_{11}, modified powder due to less amount of Pr_6O_{11}, SEM images of WC-12Co and Pr_6O_{11} modified coatings of the coated cross-section are shown in Fig. 6.3 (a-h), respectively. The coating thickness was observed to be equal to 300 ±20µm in all the specimens. White tungsten carbide grains are implanted in the back or gray in the cobalt phase. In WC-12Co, the coating coarse grain was observed, and the carbide grain was distributed widely. The addition of Pr_6O_{11} in WC-12Co coatings up to 1.2 wt. % refines the microstructure and reduces the grain size of carbide particles, as seen in Fig. 4(c-h). Further addition increases the grain size of carbide particles, resulting in an increase in the porosity of the coating, and some un-melted spots are also seen in Fig.4 (h). During coating deposition, WC grain dissolves in the melted Co phase due to the addition of high heat, resulting in the formation of small grains, and these small grain residues on the surface of the matrix increase grain growth.

Cross-sectional SEM images of coated surfaces for WC-12Co, 1Pr6O11modified, 2Pr6O11and 3Pr6O11modified coatings are shown in fig. 4(a-f) respectively. Fig. 4(a, c & e) endorse the thickness of coatings is equivalent to 300±20 µm.

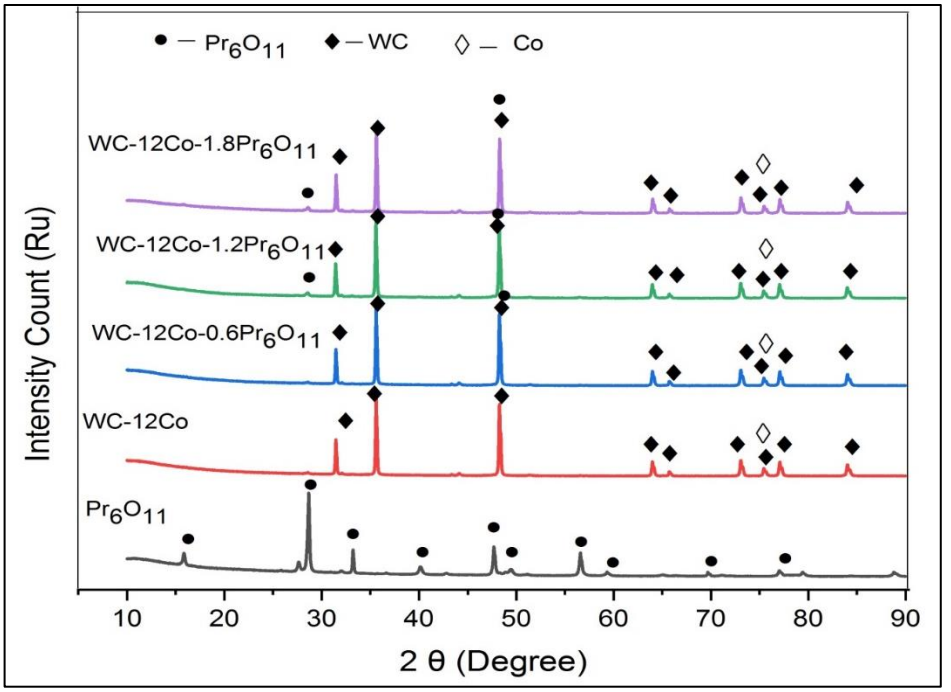

Fig. 3 XRD pattern of WC-12Co and Pr_6O_{11} modified feedstock powder

White tungsten carbide grains are implanted in the back or gray in the cobalt phase [29-30]. In WC-12Co, the coating coarse grain was observed, and the carbide grain was distributed widely. The addition of Pr_6O_{11} in WC-12Co coatings up to 1.2 wt. % refines the microstructure and reduces the grain size of carbide particles as seen in Fig. 4(c-h). Further addition increases the grain size of carbide particles, resulting in an increase in the porosity of the coating, and some un-melted spots are also seen in Fig. 4(h). It might be because the extra amount of Pr_6O_{11} causes the improvement of the sinter expanse in the matrix, which increases the grain boundary and does not get absorbed in the WC-12 Co matrix.

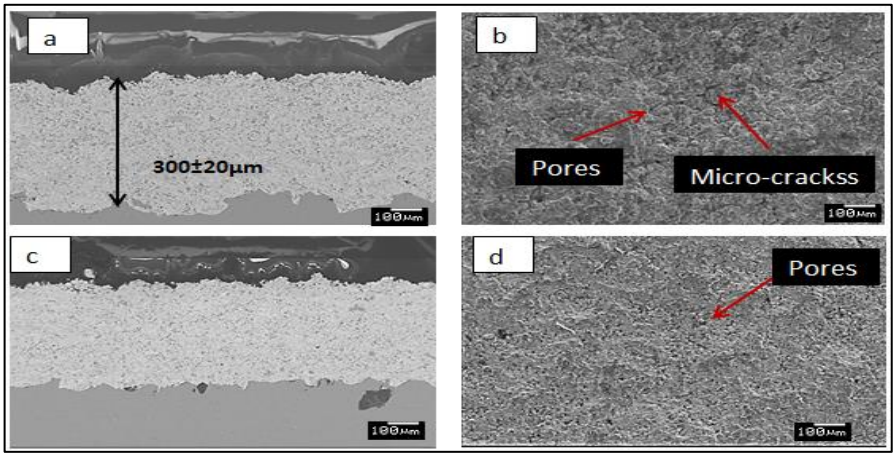

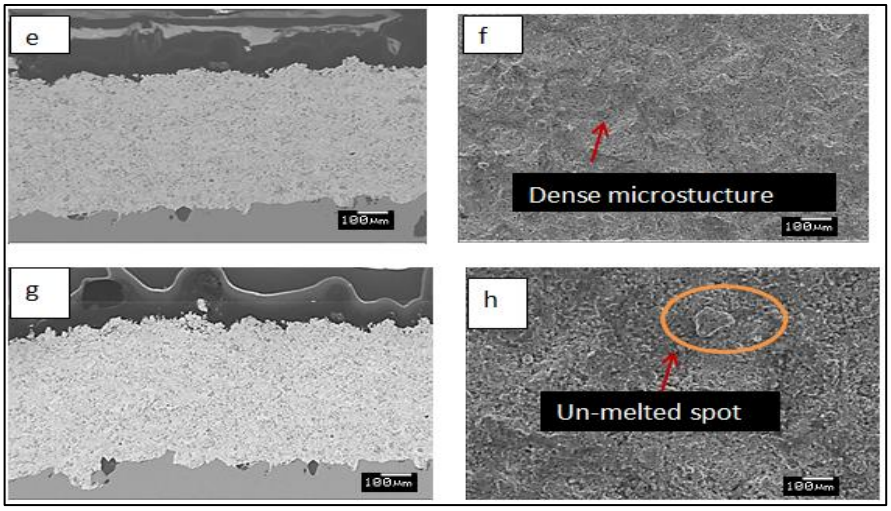

Fig. 4 SEM images of microstructure of cross-section and coated surface of WC-12Co (a & b), 1Pr6O11modified (c & d), 2Pr6O11modified (e & f) and 3Pr6O11modified (g & h) modified coatings.

During coating deposition, WC grain dissolves in the melted Co phase due to the addition of high heat, resulting in the formation of small grains, and these small grains precipitate on the surface of the matrix, which increases grain growth.

Some pores and micro-cracks were also observed on unmodified WC-12Co coating Fig. 4 (b). The addition of Pr_6O_{11} reduces the contact area between the carbide particles and prohibits the diffusion of WC grain. Therefore, it restricts the carbide grain growth and prevents the boundary segregation [31][32]. The addition of Pr_6O_{11} also endorses the dispersion of carbide particles in the Co binder phase during coating depositions to prohibit the WC particles in the matrix, restricting grain growth [33].

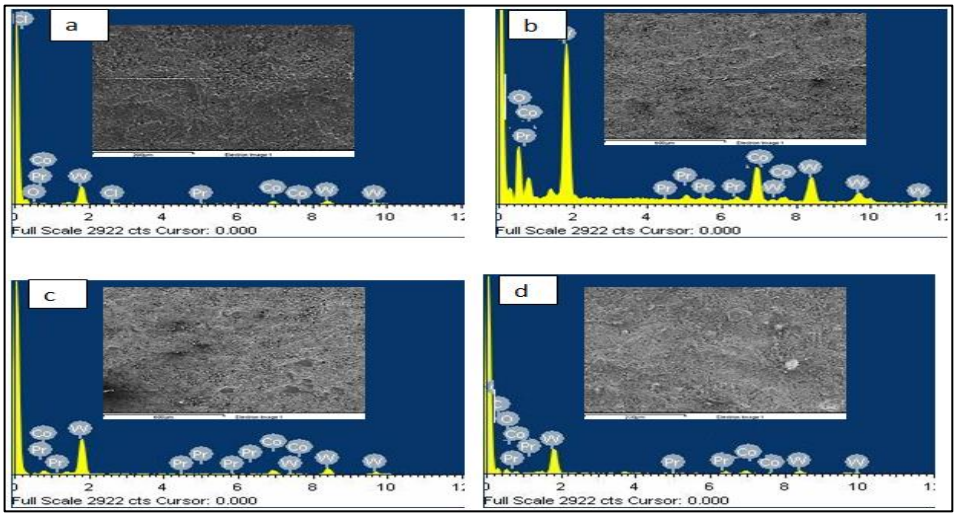

Fig. 5 EDS pattern of WC-12Co (a), 1 (b), 2 (c) and 3 Pr6O11modified (d) modified

coatings.

Fig. 5 shows an EDS graph of WC-12Co and Pr_6O_{11} modified coating and confirms the presence of various elements, including W, Co and Pr. The presence of O was also seen due to oxidation during coating deposition.

The XRD patterns of WC-12Co and Pr_6O_{11} modified coatings are shown in Fig. 6. Major peaks represent WC, and minor peaks of W_2C, Co, and Co_6W_6C are also identified. The development of the W_2C phase results from a low degree of disintegration of the WC to W_2C phase during heat addition when the coating is deposited on the surface. The formation of W_2C phase is due to the decomposition of WC into dissolved Co binder in the presence of oxygen and heat during coating deposition. W_2C is further decarburized and forms metallic WC in the presence of oxygen [34-35]. The decarburization and decomposition occur in two progressive stages [29].

$$W \rightarrow W_2C + C \quad (1)$$

$$W_2C + O_2 \rightarrow W + CO_2 \quad (2)$$

The main stage includes the development of the W2C phase because of the dispersion of W and C particles into a liquefied Co binder, and in the second step, the W2C phase is decarburized in metallic tungsten within the presence of oxygen.

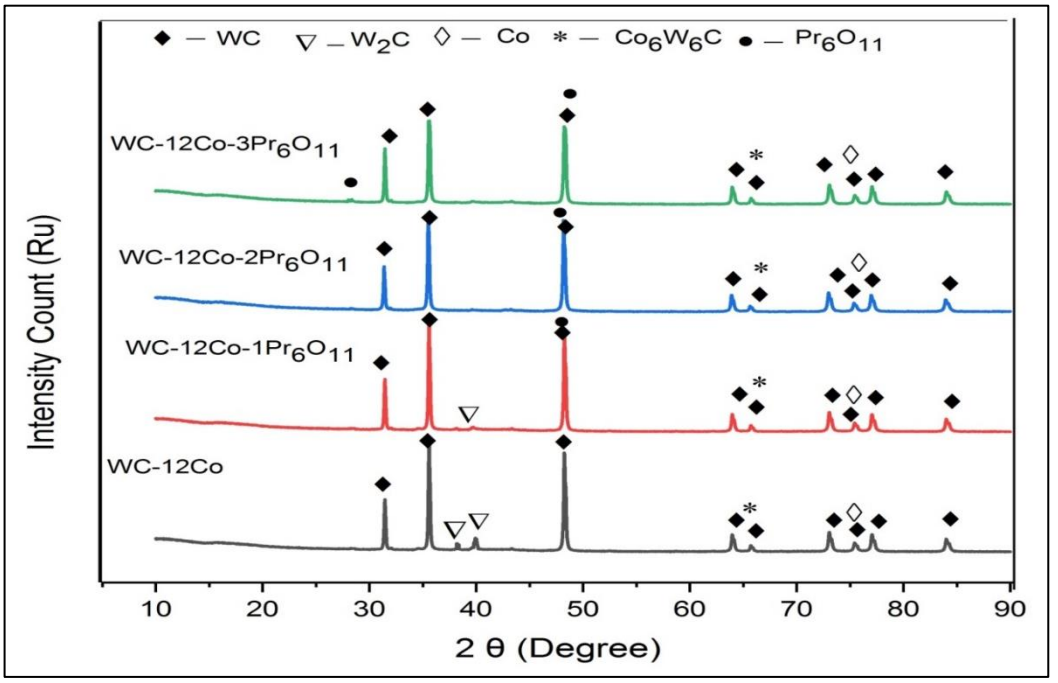

Fig. 6 XRD patterns of WC-12Co coating and Pr_6O_{11} modified coatings

Furthermore, tungsten carbide and dissolved tungsten partly react with binder phase Co, forming complex η phase Co6W6C [30]. However, the peak height of WC and W2C decreases

with the increment of Pr6O11 content. W2C (θ= 40°) disappears in WC-12Co-2Pr6O11 and WC-12Co-3Pr6O11 coatings. Similarly, W2C (θ= 38°) phase does not appear in modified coatings. The W2C phase is hard and brittle. The addition of Pr_6O_{11} restricts the decomposition and decarburization. No other peaks are seen except Pr_6O_{11}, which may be due to Pr_6O_{11} remaining intact during coating deposition at a high temperature, promoting oxidation and forming the oxide layer.

3.2 Mechanical properties

The mechanical properties of coatings are shown in Table 3 and Fig. 7. Initially, the microhardness and adhesive bond strength of coatings increase to 1.2 wt. % of Pr_6O_{11} then decreases with the increment of Pr_6O_{11}. It is observed that the porosity of the modified coating is the least in the 2Pr6O11 modified coating, which is due to its dense and refined microstructure. The Pr_6O_{11} modified coatings show higher hardness than the WC-12Co coating. Hardness increases with a decrease in grain size (addition of Pr_6O_{11} decreases grain size) hence; 2Pr6O11modified coating shows maximum hardness (1320± 90$HV_{0.3}$) as compared to other modified coating and is 7.3% higher than WC-12Co coating. Similarly, 1Pr6O11 and 3Pr6O11 modified coatings exhibited 4.1 and 2.7% higher hardness than WC-12Co coatings. Maximum adhesive bond strength is exhibited by 2Pr6O11modified coating. The adhesive bond strength of 1Pr6O11, 2Pr6O11, and 3Pr6O11modified coatings are 2.9%, 6.9%, and 2.5% higher as compared to WC-12Co coating, respectively, Minimum porosity, maximum hardness, and maximum adhesive bond strength are attributed to small grain size, dense microstructure, and restricted decarburization. The addition of rare earth elements reduces the grain size and remains on the edges of melted cobalt binder and WC, resulting in less contact between WC and flame during coating spraying [31]. Subsequently, a reduction of decarburization and new boundary formation takes place, which causes higher hardness and adhesive bond strength. The addition of Pr_6O_{11} increases the homogeneity and steadiness of the microstructure, which increases the strength of the coating. An extra addition of Pr_6O_{11} promotes the grainy cluster and enhances the separation between WC and Co phases. The excess amount of La_2O_3 also contributes to the formation of cracks. The surface roughness of all coatings is observed between 4.8 Ra (μm) to 6.3 Ra (μm).

Table 3 Mechanical Properties

Coating	Average Microhardness ($HV_{0.3}$)	Porosity (%)	Surface roughness Ra (μm)	adhesive strength (Mpa)
WC-12Co	1230± 90	1.5±0.04	6.63	68.25
WC-12Co-1 Pr_6O_{11}	1280 ±80	1.3±0.04	5.564	70.23
WC-12Co-2 Pr_6O_{11}	1320±70	0.9±0.03	4.837	72.98
WC-12Co-3 Pr_6O_{11}	1263±70	1. 1±0.03	5.741	69.96

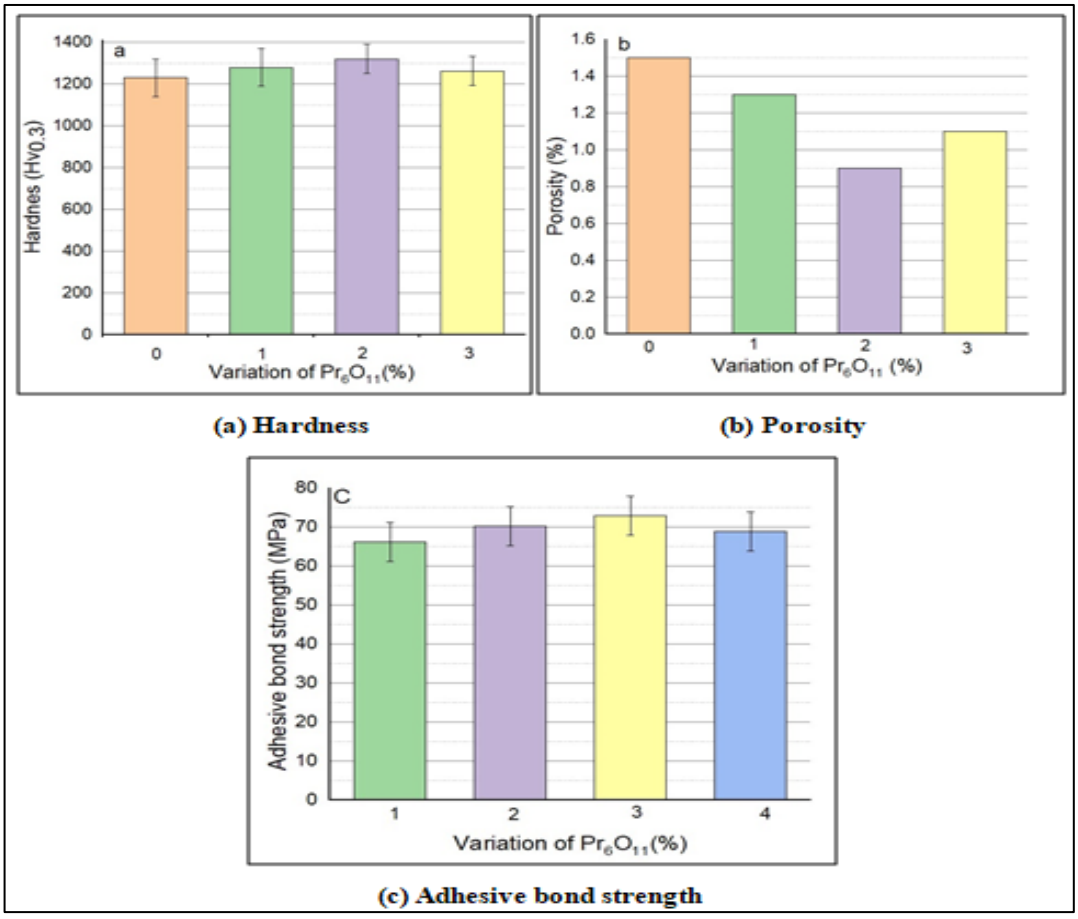

Fig. 7 Variation in (a) Hardness (b) Porosity and (c) Adhesive bond strength

3.3 Abrasive wear and coefficient of friction

The abrasive wear mass loss of WC-12Co, 1 Pr_6O_{11}, 2$Pr_6O_{11,}$ and 3 Pr_6O_{11} modified coatings at 20 N and 40 N loads are shown in Fig. 8 (a-b). It is observed that wear rate increases linearly with increments of sliding distance, and the 2Pr6O11 modified coating shows a comparatively lower mass loss than other modified coatings. Mass loss of 1 Pr_6O_{11}, 2 $Pr_6O_{11,}$ and 3 Pr_6O_{11} modified coatings are 30%, 40%, and 15% lower than the WC-12Co coating at 20N loads. Similarly, the wear rate of 1, 2, and 3Pr_6O_{11} modified coatings are 31%, 41%, and 10% lower than the WC-12Co coating at 40N loa, respectively. Mass loss of coatings at a load of 40 N is more than 1.5 times 20 N loads in all the cases. Dense microstructure, higher hardness, better bond strength, and reformation of boundaries during spraying cause the minimum mass loss of modified coatings.

Variations of the coefficient of friction (COF) of modified and unmodified coatings are shown in Fig. 9 (a-b). Initially, an increasing trend in the coefficient of friction is observed, trailed by a stable state region after 100 m sliding distance in all the cases. The coefficient of friction of 1, 2, 3 Pr_6O_{11} modified coatings and WC-12Co coatings are 0.24, 0.20, 0.27, and 0.32,

respectively, at a load of 20 N, whereas 0.39, 0.31, 0.43, and 0.48 at a load of 40 N. Minimum coefficient of friction is observed for 2 Pr_6O_{11} modified coating.

Initially, the increased trend of the coefficient of friction can be endorsed to increased shear stress between the abrasive media and asperities removed from the coated surface. As the sliding distance increases, the real contact area also increases, resulting in a decrease in shear stress. A sudden increment in friction force due to the implanting of abrasive particles in a softer Co binder and the removal of carbide particles may be another reason for the higher coefficient of friction [32]. The temperature between the interfaces of the contact zone continuously increases, and carbide particles stick to coated surfaces due to adhesion, resulting in the formation of tribo oxide layer, which reduces the coefficient of friction. The addition of Pr_6O_{11} enhances the formation of the oxide layer. Therefore, modified coatings have a comparatively lower coefficient of friction than unmodified WC-12Co coating. The other reason for the lower coefficient of friction of modified coating is the self-lubricant properties of rare earth elements; therefore, 3% modified Pr6O11 coating exhibited a minimum coefficient of friction.

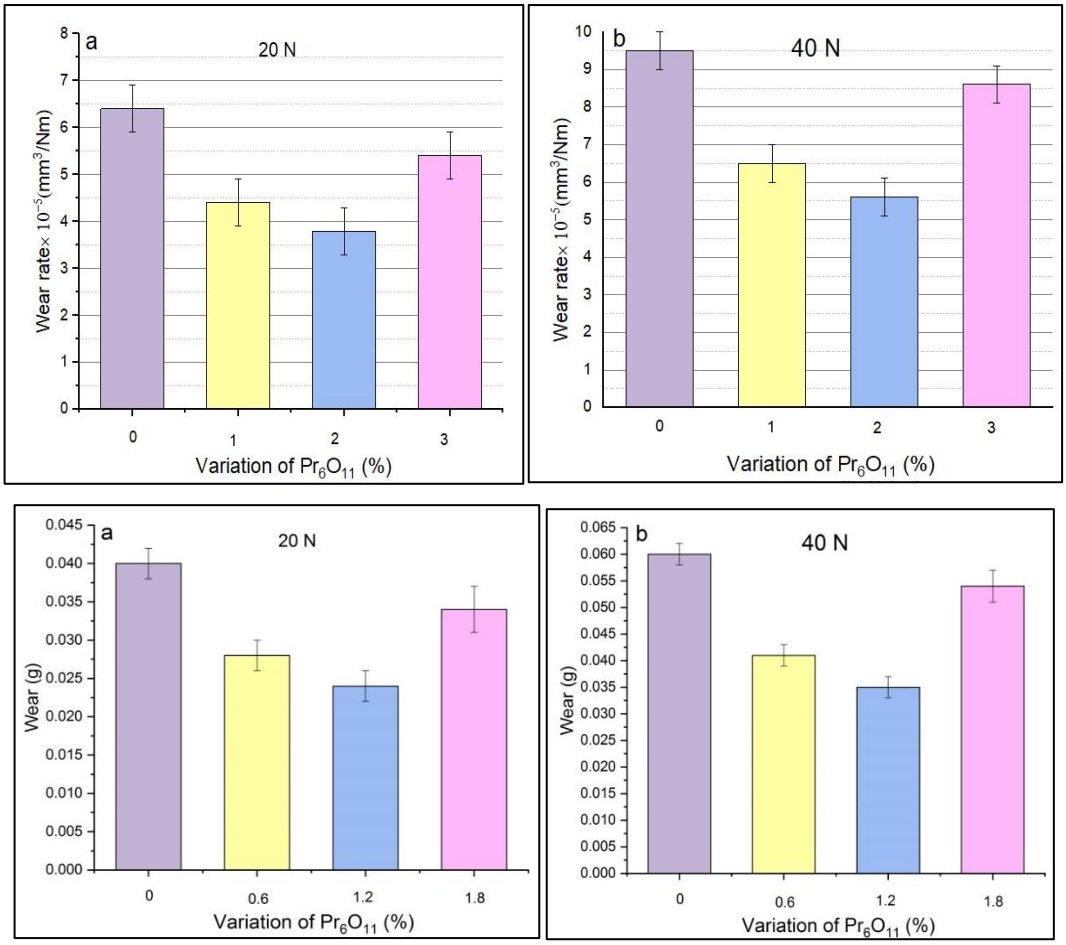

Fig. 8 Variation in mass loss at load of (a) 20 N (b) 40 N.

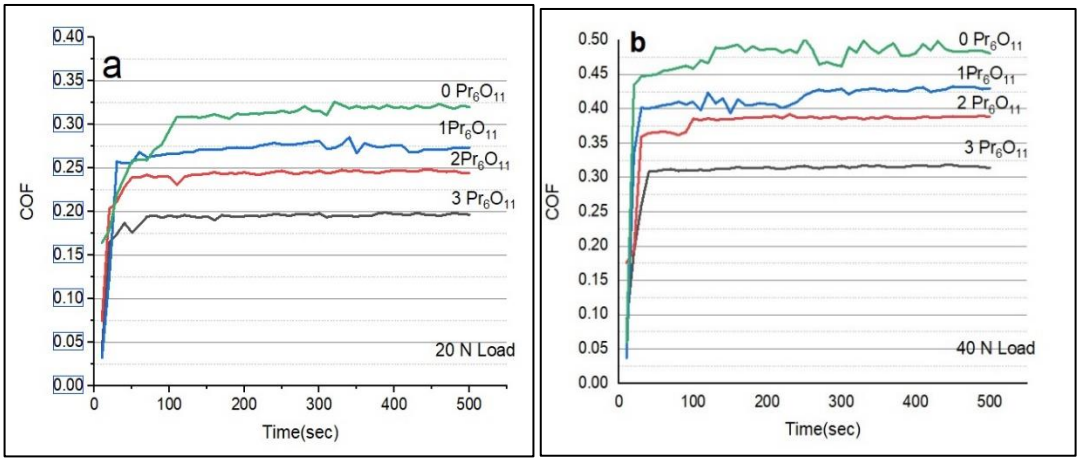

Fig. 9 Variation in the coefficient of friction at a load of (a) 20 N (b) 40 N.

3.4 Worn Surface Analysis

Wear mechanisms of worn-out surfaces of WC-12Co and Pr6O11 modified coatings were investigated using SEM images as shown in Fig. 10(a-f). at the load of 20 and 40 N.

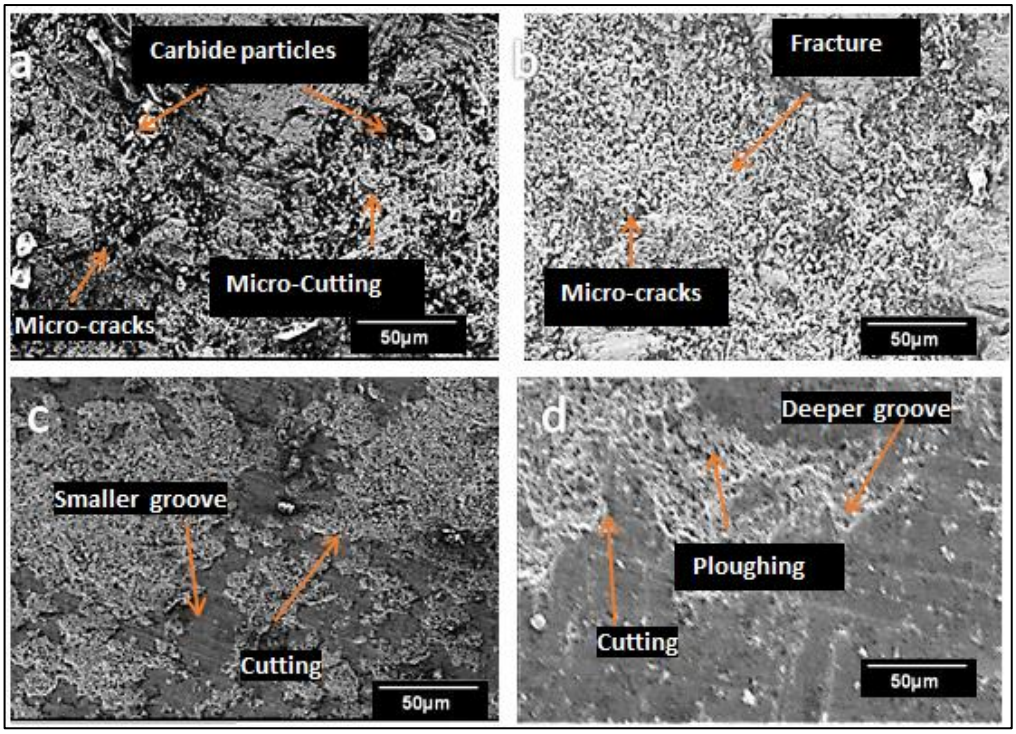

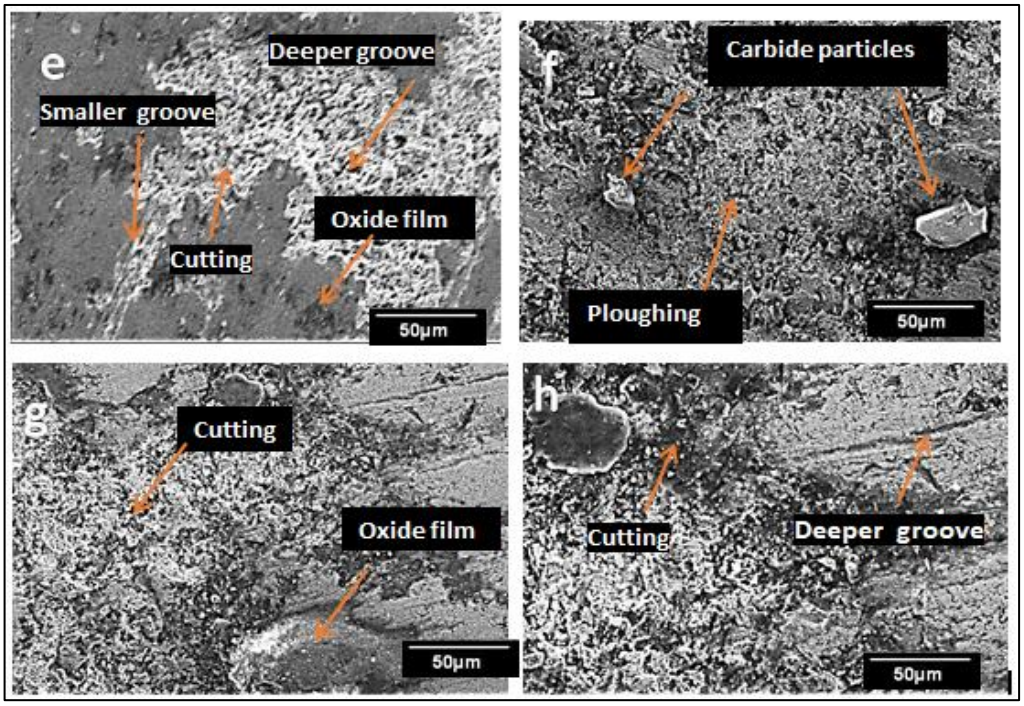

Fig. 10 microstructure of worn-out surface at 20 and 40 N load of the (a-b) WC-12Co, (c-d) 0.6 Pr_6O_{11}, (e, f) 1.2 Pr_6O_{11} and (g, h) 1.8 Pr_6O_{11} modified coating

The 2 Pr_6O_{11} modified coating reveals superior wear properties than other coatings due to its comparatively minimum grain size, higher microhardness, and better adhesive bond strength. Higher wear is observed at 40 N load and is attributed to deeper and wider grooves created by angular-shaped silicon carbide particles, which remove a comparatively higher fraction of material. Ploughing and cutting wear mechanisms are observed in modified coatings at lower and higher loads. In Pr_6O_{11} modified coatings, the oxide film formed due to high heat generation during sliding, preventing further wear. It was also observed that Pr_6O_{11} modified coatings also prevent cracks, and no cracks were seen in Pr_6O_{11} modified coatings. Displacement of carbide particles, micro-cracks, and delamination are noticed in WC-12Co coating at 20N load, as shown in Fig. 10 (a). Delamination, micro-cracks, and fracture dominate the wear mechanism in WC-12Co coating at 40 N load, as seen in Fig. 10 (b).

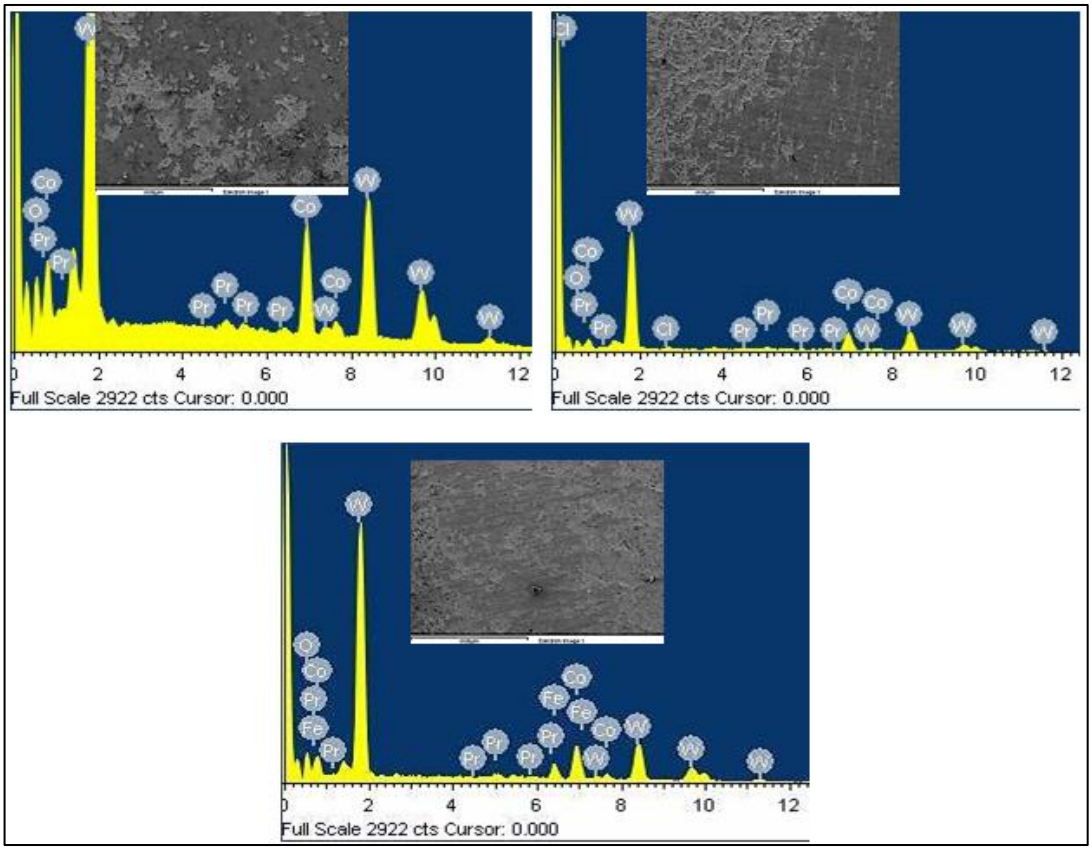

Fig. 11 EDS analysis of worn out surfaces of coatings (a) WC-12Co-1Pr_6O_{11} (b) WC-12Co-2Pr_6O_{11} (c) WC-12Co-3Pr_6O_{11} at 40N

Abrasive wear strongly depends on the binder mean free path, the grain size of coating particles, and the proportion of hard and binder phases [33]. The addition of Pr_6O_{11} reduces the grain size, restricts boundary segregation, and promotes the oxide layer, resulting in minimum wear noticed in modified coatings. The EDS result of modified coatings shows the existence of Pr, W, Co along with oxygen, which confirms the presence of a tribo oxide layer as shown in Fig. 11(a-c).

4. Conclusions

Following conclusions can be drawn from the present investigation:

(1) The addition of Pr_6O_{11} extensively restricts the irregular growth of WC grain, refines the microstructure, and reduces the crack formation and porosity.

(2) The formation of the undesired W_2C phase is due to decarburization and is responsible for brittleness, which is prevented by the addition of Pr_6O_{11}.

(3) The addition of Pr_6O_{11} enhances the microhardness adhesive bond strength of coatings up to 2 wt. %. only. WC-12Co exhibits maximum microhardness and adhesive bond strength-$2Pr_6O_{11}$ having values of 1320 ±70$HV_{0.3}$ and 72.98 Mpa, respectively 7.3% and 6.9 % higher than WC-12Co coating.

(4) Optimum addition of 2 wt. % shows the minimum wear rate 40% lower than the unmodified WC-12Co coating.

(5) The addition of Pr_6O_{11} promotes the formation of the tribo oxide layer, which reduces the coefficient of friction.

(6) Investigation of the worn-out surface of the WC-12Co coating and modified coatings shows that a ploughing and cutting wear mechanism is observed in modified coatings. Delamination and micro-cutting mechanisms are seen in WC-12Co coating in both 40N and 60 N loads.

Highlights

- The addition of Pr_6O_{11} reduces the grain size of WC particles, thus refining the microstructure.
- Pr6O11 exclusively restricts the decarburization of WC-12Co coating.
- Optimum addition of 1.2 wt. % Pr_6O_{11} shows higher hardness and adhesive bond strength.
- Minimum mass loss was observed by 1.2 Pr_6O_{11} coating.
- The cutting and ploughing wear mechanism is noticed with the addition of Pr_6O_{11} in WC-12Co coating.

References

[1] T.N. Rhys-Jones, The use of thermally sprayed coatings for compressor and turbine applications in aero engines, Surf. Coatings Technol. 42 (1990) 1–11. https://doi.org/10.1016/0257-8972(90)90109-P.

[2] Z. Geng, S. Hou, G. Shi, D. Duan, S. Li, Tribological behaviour at various temperatures of WC-Co coatings prepared using different thermal spraying techniques, Tribol. Int. 104 (2016) 36–44. https://doi.org/10.1016/j.triboint.2016.08.025.

[3] M. Xie, S. Zhang, M. Li, Comparative investigation on HVOF sprayed carbide-based coatings, Appl. Surf. Sci. 273 (2013) 799–805. https://doi.org/10.1016/j.apsusc.2013.03.010.

[4] N. Ma, L. Guo, Z. Cheng, H. Wu, F. Ye, K. Zhang, Improvement on mechanical properties and wear resistance of HVOF sprayed WC-12Co coatings by optimizing feedstock structure, Appl. Surf. Sci. 320 (2014) 364–371. https://doi.org/10.1016/j.apsusc.2014.09.081.

[5] S. Hong, Y. Wu, B. Wang, Y. Zheng, W. Gao, G. Li, High-velocity oxygen-fuel spray parameter optimization of nanostructured WC-10Co-4Cr coatings and sliding wear behavior of the optimized coating, Mater. Des. 55 (2014) 286–291. https://doi.org/10.1016/j.matdes.2013.10.002.

[6] A. Mateen, G.C. Saha, T.I. Khan, F.A. Khalid, Tribological behaviour of HVOF sprayed near-nanostructured and microstructured WC-17wt.%Co coatings, Surf. Coatings Technol. 206 (2011) 1077–1084. https://doi.org/10.1016/j.surfcoat.2011.07.075.

[7] M.G. Gee, A. Gant, B. Roebuck, Wear mechanisms in abrasion and erosion of WC/Co and related hardmetals, Wear. 263 (2007) 137–148. https://doi.org/10.1016/j.wear.2006.12.046.
[8] C.J. Li, A. Ohmori, Y. Harada, Effect of powder structure on the structure of thermally sprayed WC-Co coatings, J. Mater. Sci. 31 (1996) 785–794. https://doi.org/10.1007/BF00367900.
[9] H. Wang, Y. Li, M. Gee, H. Zhang, X. Liu, X. Song, Sliding wear resistance enhancement by controlling W2C precipitation in HVOF sprayed WC-based cermet coating, Surf. Coatings Technol. 387 (2020) 125533. https://doi.org/10.1016/j.surfcoat.2020.125533.
[10] B. Trindade, M.T. Vieira, E. Bauer-Grosse, Amorphous phase forming ability in (W-C)-based sputtered films, Acta Mater. 46 (1998) 1731–1739. https://doi.org/10.1016/S1359-6454(97)00336-4.
[11] P.H. Shipway, D.G. McCartney, T. Sudaprasert, Sliding wear behaviour of conventional and nanostructured HVOF sprayed WC-Co coatings, Wear. (2005). https://doi.org/10.1016/j.wear.2005.02.059.
[12] F. Zhang, A. Tabecki, M. Bennett, H. Begg, S. Lionetti, S. Paul, Feasibility Study of High-Velocity Oxy-fuel (HVOF) Sprayed Cermet and Alloy Coatings for Geothermal Applications, J. Therm. Spray Technol. 32 (2023) 339–351. https://doi.org/10.1007/s11666-023-01559-5.
[13] H. Zhou, F. Zhu, G. Ma, C. Xue, Y. Hu, Effect of nano rare earth on corrosion resistance of thermal sprayed WC/12Co coating, Surf. Rev. Lett. 25 (2018) 1–11. https://doi.org/10.1142/S0218625X18501147.
[14] Y. Liu, G. Gou, X. Wang, Q. Jia, H. Chen, M. Tu, Effects of Rare Earth Elements on the Microstructure and Mechanical Properties of HVOF-Sprayed WC-Co Coatings, J. Therm. Spray Technol. 23 (2014) 1225–1231. https://doi.org/10.1007/s11666-014-0072-7.
[15] C. SHI, Z. JIN, H. REN, J. YOU, Effect of lanthanum on recrystallization behavior of non-oriented silicon steel, J. Rare Earths. 35 (2017) 309–314. https://doi.org/10.1016/S1002-0721(17)60914-1.
[16] C. Wu, M. Ma, W. Liu, M. Zhong, H. Zhang, W. Zhang, Laser cladding in-situ carbide particle reinforced Fe-based composite coatings with rare earth oxide addition, J. Rare Earths. 27 (2009) 997–1002. https://doi.org/10.1016/S1002-0721(08)60377-4.
[17] Y. Lian, L. Yu, Q. Xue, The effect of cerium dioxide on the friction and wear properties of flame spraying nickel-based alloy coating, Wear. 181–183 (1995) 436–441. https://doi.org/10.1016/0043-1648(95)90052-7.
[18] D. Shu, S. Dai, G. Wang, W. Si, P. Xiao, X. Cui, X. Chen, Influence of CeO2 content on WC morphology and mechanical properties of WC/Ni matrix composites coating prepared by laser in-situ synthesis method, J. Mater. Res. Technol. 9 (2020) 11111–11120. https://doi.org/10.1016/j.jmrt.2020.07.104.
[19] Y. Liu, Z. Hang, G. Yang, H. Fu, N. Xi, H. Chen, Influence of Rare Earth on the High-Temperature Sliding Wear Behavior of WC-12Co Coating Prepared by HVOF Spraying, J. Therm. Spray Technol. 27 (2018) 1143–1152. https://doi.org/10.1007/s11666-018-0764-5.
[20] M. Zhang, S. Ma, K. Xu, P.K. Chu, Corrosion resistance of praseodymium-ion-implanted TiN coatings in blood and cytocompatibility with vascular endothelial cells, Vaccum. 117 (2015) 73–80. https://doi.org/10.1016/j.vacuum.2015.04.014.
[21] Kang, E. Fischer, Traugott Jia, Sliding wear of conventional and nanostructured cemented carbides, Wear. 203–204 (1997) 310–318. https://doi.org/10.1016/S0043-1648(96)07423-6.
[22] A. Evans, T.W.-A. Metallurgica, undefined 1976, Quasi-static solid particle damage in brittle solids—I. Observations analysis and implications, Elsevier. (n.d.). https://www.sciencedirect.com/science/article/pii/0001616076900420 (accessed April 4, 2020).
[23] H. Wang, X. Wang, X. Song, X. Liu, X. Liu, Sliding wear behavior of nanostructured WC-Co-Cr coatings, Appl. Surf. Sci. 355 (2015) 453–460. https://doi.org/10.1016/j.apsusc.2015.07.144.
[24] M. Afzal, M. Ajmal, A. Nusair Khan, Wear behavior of WC-12%co coatings produced by air plasma spraying at different standoff distances, Tribol. Trans. 57 (2013) 94–103.

https://doi.org/10.1080/10402004.2013.850763.
[25] Z. Pan, T. Wang, L. Chen, S. Idziak, Z. Huang, B. Zhao, Effects of Rare Earth Oxide Additive on Surface and Tribological properties of, Appl. Surf. Sci. (2017). https://doi.org/10.1016/j.apsusc.2017.04.172.
[26] G. Yuxin, Y. Jian, Effect of La2O3 addition on microstructure and wear behavior of electrospark deposited Ni-based coatings, Surf. Rev. Lett. 20 (2013). https://doi.org/10.1142/S0218625X13500601.
[27] A. Mechanics, Study on Pr 6 O 11 –doped superfine-grained WC–Co cemented carbides Wang Jun 1, 529 (2014) 57–61. https://doi.org/10.4028/www.scientific.net/AMM.529.57.
[28] P. Chivavibul, M. Watanabe, S. Kuroda, K. Shinoda, Effects of carbide size and Co content on the microstructure and mechanical properties of HVOF-sprayed WC-Co coatings, Surf. Coatings Technol. 202 (2007) 509–521. https://doi.org/10.1016/j.surfcoat.2007.06.026.
[29] C.J. Li, A. Ohmori, K. Tani, Effect of WC particle size on the abrasive wear of thermally sprayed WC-Co coatings, Mater. Manuf. Process. 14 (1999) 175–184. https://doi.org/10.1080/10426919908914815.
[30] H.O. Andrén, U. Rolander, P. Lindahl, Atom-probe analysis of cemented carbides and cermets, Appl. Surf. Sci. 76–77 (1994) 278–284. https://doi.org/10.1016/0169-4332(94)90355-7.
[31] Z. Zhang, X. Lu, B. Han, J. Luo, Rare earth effect on microstructure, mechanical and tribological properties of CoCrW coatings, Mater. Sci. Eng. A. 444 (2007) 92–98. https://doi.org/10.1016/j.msea.2006.08.091.
[32] M. Mohanty, R. Smith, M. De Bonte, J.C.- Wear, undefined 1996, Sliding wear behavior of thermally sprayed 75/25 Cr3C2/NiCr wear resistant coatings, Elsevier. (n.d.). https://www.sciencedirect.com/science/article/pii/0043164896069839 (accessed April 4, 2020).
[33] S. Usmani, S. Sampath, D.L. Houck, D. Lee, Effect of carbide grain size on the sliding and abrasive wear behavior of thermally sprayed WC-Co coatings, Tribol. Trans. 40 (1997) 470–478. https://doi.org/10.1080/10402009708983682.